Bulletin of the Seismological Society of America, Vol. 97, No. 3, pp. 989–1001, June 2007, doi: 10.1785/0120060136

Identification of Delay-Fired Mining Explosions Using Seismic Arrays: Application to the PDAR Array in Wyoming, USA

by Stephen J. Arrowsmith,* Michael A. H. Hedlin, Marie D. Arrowsmith, and Brian W. Stump

Abstract We extend a time-frequency discrimination algorithm, developed in an earlier article (Arrowsmith *et al.*, 2006), for application to seismic-array data. Spectrograms evaluated at each component of an array are stacked and then converted into binary form for computation of discriminants. Because noise can bias the discriminants, we develop a procedure for removing the effect of noise on the discriminants. The binary spectrograms are randomized where the spectral amplitude of the signal is similar to the mean spectral amplitude of the pre-event noise at that frequency. The formulism of Arrowsmith *et al.* (2006) is further extended by modifying the objective function used to optimize the values of input parameters and by removing high-frequency and low-frequency spectral content. We apply the method to a dataset of regional recordings of earthquakes and delay-fired mine blasts recorded at the Pinedale seismic array in Wyoming. Our results show that the utilization of array data improves the success rate for source identification. Furthermore, we find that incorporating the noise-correction procedure increases the separation between earthquakes and cast overburden blasts (the largest type of delay-fired mine blasts). In total, the algorithm successfully identifies 97.4% of the events (74 of a total of 76 events, which comprise earthquakes and cast overburden blasts).

Introduction

The establishment of the International Monitoring System (IMS) for nuclear explosion monitoring has led to increased interest in discriminating small (m_b <4.0) seismic events, of which mining events are prolific. This has resulted in the need for regional discrimination techniques that can separate not only earthquakes and single-fired explosions, but also delay-fired mining explosions. Most existing regional discrimination techniques are based on single-station measurements and do not exploit the supplementary information on the seismic wave field that is inherent in array data, despite the fact that there are 35 arrays (including both planned and existing arrays) in the IMS. In a previous article (Arrowsmith *et al.*, 2006), hereafter referred to as "article 1," we developed a fully automatic technique for identifying delay-fired mine blasts in regional seismic datasets. In this article we extend the methodology described in article 1 for application to array data.

Seismic arrays permit significant improvements in seismic signal-to-noise ratios, which can lower detection thresholds. By stacking waveforms recorded at individual array elements, coherent signal is amplified with respect to relatively incoherent noise. Thus, seismic-array data are used in event detection algorithms (e.g., Bungum and Husebye, 1974; Ringdal *et al.*, 1975; Cansi, 1995). In addition to enhancing the signal-to-noise level, seismic arrays can allow the association of phase velocities and backazimuths with arrivals. This has led to the use of seismic-array data in phase identification (e.g., Mykkelveit and Ringdal, 1981) and in earthquake location algorithms (e.g., Bratt and Bache, 1988; Ringdal and Husebye, 1982). Despite the utility of array data for these applications, seismic-array data are not used routinely in seismic-event discrimination. Examples where array data have been utilized include a few regional and teleseismic studies. Dysart and Pulli (1990) stack spectra from the different elements of the NORESS seismic array to compute both frequency- and amplitude-based discriminants. Baumgardt and Young (1990) use incoherent beamforming and compute frequency- and amplitude-based discriminants at the NORESS array. Hedlin *et al.* (1990) stack binary spectrograms computed for each element of the NORESS array to enhance time-independent spectral banding. Taylor and Marshall (1991) use beamforming and spectral stacking to compute amplitude ratios for data from four teleseismic arrays. Shumway *et al.* (1998) study data from the ARCESS seismic array and stack spectra from each separate component of the array to discriminate delay-fired seismic signals from other types of event. However, none of these studies

*Present address: Los Alamos National Laboratory, EES-2, P.O. Box 1663, MS D401, Los Alamos, New Mexico 87545; sarrowsmith@gmail.com.

directly compared the resultant array result with the result obtained using a single station only.

The method described in article 1 exploits the fact that delay-fired mining explosions give rise to seismic waveforms that possess highly colored spectra (i.e., spectra enriched in power at certain frequency bands and depleted in power in others). Such spectral modulations do not vary with time in the recorded waveforms (Hedlin *et al.*, 1989). At regional distances, in the bandwidth sampled by most seismometers, spectral modulation is thought to arise from either (1) the constructive interference of seismic waves from adjacent rows in a typical explosion shot pattern (which are detonated with the same interrow delays), or (2) by the duration of the blast sequence (Hedlin *et al.*, 1990; Chapman *et al.*, 1992). For more information on the causes of spectral modulation, see the discussion in the following. Because nuclear explosions are not typically delay fired, although this would be theoretically possible, the identification of events that possess time-independent spectral modulations is a useful tool in nuclear monitoring. In addition to the technique described in article 1, spectral modulations have been exploited by Baumgardt and Ziegler (1988), Hedlin *et al.* (1989, 1990), Dysart and Pulli (1990), Shapira *et al.* (1996), Gitterman *et al.* (1998), Hedlin (1998), and Shumway *et al.* (1998) for the identification of delay-fired mine explosions.

In this article, we first extend the methodology described in article 1 for application to array data. We also discuss the effect of noise on the results and introduce a procedure for correcting for this. Next, the time-frequency discriminant is applied to the Pinedale seismic array in Wyoming. We summarize our results to assess the benefit of utilizing the data from the full array over a single station only.

Methodology

Article 1 describes a fully automatic methodology for the identification of delay-fired mining explosions in regional seismic datasets. Rather than discriminating among two or more possible event classes, the technique can identify simply whether an event is a delay-fired mining explosion. As discussed in article 1, the technique can provide seven separate discriminants based on the binary spectrograms of seismic events recorded at a three-component seismograph. The seven discriminants include the cepstral mean, the three values of cross-correlation of the binary spectrograms evaluated on all three components, and the three values of autocorrelation of the binary spectrograms on each component separately. For more details on the method used for evaluating these discriminants, the reader is referred to article 1. In brief, to calculate the cepstral mean, a 2D cepstral matrix is evaluated by taking the 2D Fourier transform of the binary spectrograms. Next, the columns of the 2D cepstral matrix, which represent energy that is periodic in frequency and independent of time, are stacked for each perpendicular component. The mean value of this 1D-stacked cepstrum is evaluated by using a window that includes the first few cepstral values (the length of the cepstral window is optimized as described subsequently). Cross-correlation coefficients are evaluated for each pair of 2D binary spectrograms (recorded on each component) to provide discriminants that exploit the fact that spectral modulations are a source property, hence independent of recording direction. Finally, autocorrelations (as a function of lag time) of each 2D binary spectrogram are evaluated to provide discriminants that exploit the time independence of spectral modulations. For a single-component seismograph, only two separate discriminants are computed (cepstral mean and autocorrelation on the vertical component). For any given station, the algorithm can be tuned effectively with a reference set of events to maximize the success rate in identifying delay-fired and non-delay-fired events. This is accomplished by searching for the optimum values of four free parameters that maximize the separation between the two classes of reference events by using the mean Mahalanobis distance. An inherent assumption in this approach is that the nature of delay-fired blasting in a particular area does not vary significantly and that delay times between individual shots and rows in blasting arrays are similar. Otherwise it could be possible that a single optimum set of input parameters would not exist, as the optimum parameters would be different for each source.

In this article we discuss the modifications that have been made to the algorithm described in article 1, which include the following: (1) a procedure to correct for the effect of pre-event noise; (2) a modification of the computation of binary spectrograms that incorporates the removal of high-frequency and low-frequency spectral content; (3) a modification of the optimization algorithm that uses the percentage of correctly identified events, rather than the mean Mahalanobis distance between both classes of events as the objective function; and finally, (4) a technique for utilizing array data. In this article, we focus on the approach for single-component stations and then apply the methodology to an array of predominantly single-component seismometers. Therefore, we will focus on only two discriminants (mean cepstrum and autocorrelation on the single component), rather than the seven discriminants applied in article 1.

Noise Correction

White noise is associated with a flat spectrum, containing approximately equal power at all frequencies. The effect of such noise on the resultant stacked binary spectrograms (refer to article 1 for further discussion on the computation of binary spectrograms), computed for the full 15-element Pinedale array (PDAR), results in a random pattern of values for adjacent pixels. The corresponding values of the discriminants (obtained for a sample of 50 stacked white-noise spectrograms) are very low (Fig. 1), and provide a reference value for the discriminants in the case of no time-independent spectral modulations. White noise, however,

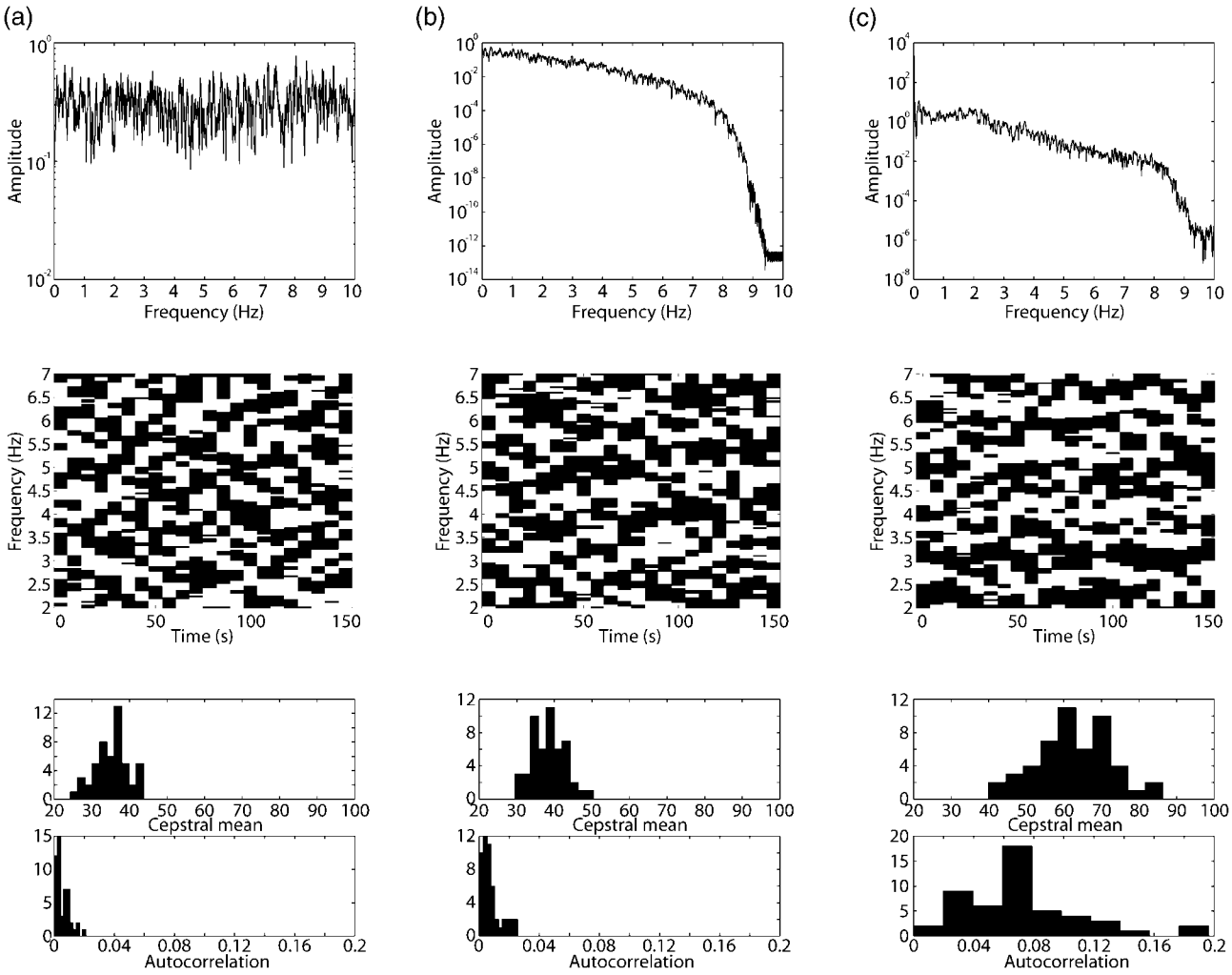

Figure 1. Figure showing the effect of noise on the binary spectrograms and resultant discriminants for synthetic white noise (left panel) (a), synthetic colored noise (center panel) (b), and real pre-event noise (right panel) (c). (Top row) Amplitude spectra of sample noise waveforms for each of the three cases (a)–(c). (Middle row) Binary spectrograms computed from 15 stacked spectrograms, each computed for a noise waveform representing a single-array element. (Bottom row) Histograms of discriminants obtained (cepstral mean and autocorrelation) from a sample of 50 noise waveforms. Note that each discriminant represents the corresponding noise value for the full array (15 elements).

does not adequately represent the typical frequency content of real noise observed at the elements of PDAR (e.g., Fig. 1). To simulate better the observed noise at PDAR, we have generated synthetic colored noise by sequentially applying two zero-phase low-pass Butterworth filters (with low-pass cutoffs at 3 Hz and 8 Hz, and orders of 1 and 3, respectively) to synthetic white noise (Fig. 1). The discriminants obtained for the sample of synthetic colored noise are similar to values obtained for the white noise (Fig. 1). However, we have found that real pre-event noise observed at PDAR typically results in low-magnitude spectral modulations. These spectral modulations are visually apparent in the associated stacked binary spectrograms, and result in an increase in the values of the discriminants (Fig. 1). Note that the discriminants plotted in Figure 1 are obtained after stacking of 15 separate spectrograms (refer to subsequent discussion on stacking), each representing a different array element. The discriminants evaluated for the pre-event noise using a single trace only (i.e., no array stacking) are significantly lower than the results shown in Figure 1 for the stacked pre-event noise. This indicates that a significant component of noise observed at the PDAR array is coherent at all the array elements. This time-independent spectral banding, which is present in the noise, may arise from a range of effects including atmospheric storms (Withers *et al.*, 1996), microseisms (Friedrich *et al.*, 1998), cultural sources (e.g., Douze and Laster, 1979), and propagation effects (Sereno and Orcutt, 1985).

Clearly it is important, in the context of developing a discriminant based on time-independent banding in binary spectrograms, to correct for the effect of noise on the results. We are interested in the presence (or absence) of banding due to source effects, and therefore it is important to remove any banding that may arise due to other effects. Therefore, we extend the methodology described in article 1 by correcting for any time-independent banding present in a sample of pre-event noise. To do this, we incorporate an additional test in our algorithm for converting spectrograms into binary form. First, we compute a spectrogram of the pre-event noise and evaluate the mean scaled logarithm of the pre-event spectrogram in each frequency band ($\bar{x}_{f(\text{pre})}$). Next, we compute the following parameter for each pixel in the spectrogram of the signal:

$$\alpha = |x_{tf} - \bar{x}_{f(\text{pre})}|, \quad (1)$$

where x_{tf} is the scaled logarithm of the signal spectrogram at time t and frequency f. We then randomize the pixels in the binary spectrogram where $\propto$ is less than some threshold. The threshold is set as a fifth input parameter to be trained to a particular dataset (refer to the following discussion for more details on optimizing the values of the input parameters).

Limitation of Bandwidth

For the application of this technique to short-period seismographs, we must consider the effect of the instrument response and the antialiasing filter. The data used in this study were acquired using Geotech 23900 seismometers with a sampling rate of 20 Hz and an antialiasing filter at 8 Hz. The sampling rate is lower than the sampling rate of the single broadband sensor used in article 1, a feature common to arrays as the coherence between array elements limits the highest frequencies that can be used for beamforming. The velocity-amplitude response is approximately flat between 2 and 7 Hz. The low-frequency and high-frequency edge effects distort the spectral content and can result in time-independent spectral banding at low and high frequencies (where the amplitude response is not flat). We have experimented with applying an instrument correction, but this causes significant amplification of noise (in addition to signal) at low and high frequencies. Therefore, we simply remove low-frequency and high-frequency content from the spectrograms. In this study we compute spectrograms for the frequency range from 2 to 7 Hz.

The frequency range considered in this article is clearly narrow band, placing restrictions on the scale of spectral modulations that can be observed. Specifically, we cannot clearly observe spectral modulations with a width (i.e., distance between spectral peaks) greater than 5 Hz. Consider what this implies in terms of the nature of the causative physical processes giving rise to the spectral modulations, and which types of process we can observe with such a limited bandwidth. As discussed in Smith (1989) and Chapman *et al.* (1992), the delay times between shots and successive rows in a blast sequence result in spectral peaks at multiples of the "comb" frequency (i.e., at multiples of $1/dt$, where dt is the intershot or interrow delay time). To cause clear and stable spectral modulations in seismic signals it is necessary that the delay times are consistent, with a small variance of raw charge weights (e.g., Gitterman and van Eck, 1993). For the events in this study, dt is $\sim$10 msec for the intershot times and $\sim$200–1100 msec for the interrow times (Table 1). These values appear to be similar in different studies also (e.g., Chapman *et al.* [1992] report intershot delay times of 9 msec and interrow delay times of 200 msec in Kentucky). As discussed in Langefors and Kihlstrom (1978), intershot delay times used in surface-mining practices are typically of the order of 20–30 msec. The intershot times in this study result in spectral modulations at intervals of $\sim$100 Hz, clearly outside the bandwidth of typical seismic data. However, interrow times imply spectral modulations with widths of 0.9–5 Hz (observable within the bandwidth considered here). Another important effect is the total duration of each mining explosion, analogous to the application of a boxcar function in the time domain. This effect causes spectral minima at multiples of $1/t_n$ (where t_n is the total duration of the blast sequence), an effect termed "spectral scalloping" by Chapman *et al.* (1992). Our 2- to 7-Hz band-limited data would imply that we could detect spectral scalloping from shot sequences with durations greater than 0.2 sec. The total durations of the shots in this study are all greater than 0.2 sec (Table 1). Clearly, the 2- to 7-Hz frequency band allows us to detect spectral modulations associated with both interrow delay times and shot sequence duration in this region.

Modification of Optimization Algorithm

In article 1 we outlined a procedure for choosing the values of four input parameters to optimize the separation between delay-fired and non-delay-fired events, where the objective function was the mean Mahalanobis distance between the two classes of events. In the application to real data, more earthquakes were misclassified than cast blasts (which are a type of delay-fired event). This bias was due to the greater variance of discriminants for the cast blast population, which downward biased the Mahalanobis distances of earthquakes from the cast blast population (article 1). In this article, we introduce an alternative approach, where the objective function to be optimized is now the percentage of correctly identified events. Figure 2 illustrates the difference between the objective function used in article 1, and the new objective function introduced in this article. In this article, we evaluate the percentage of events that are correctly classified for each selection of input parameters. For N events, we perform N iterations, where each successive event is

Table 1
Ground-Truth Information on the 33 Cast Blasts Used in This Study

Event No.	Origin Date / Time	Yield (lbs)	Intershot Delay (msec)	Interrow Delay (msec)	No. Shots	No. Rows
1	1/03/2004 (003) 19:05:00.000	677248	9	0,200,300,300,300	124	5
2	1/11/2004 (011) 18:59:59.999	1244864	9	0,200,300,300,300	229	5
3	1/16/2004 (016) 21:06:24.236	377134	9	0,200,300,300,300	67	5
4	1/17/2004 (017) 21:04:29.247	1400000	No Information	No Information	No Information	No Information
5	1/24/2004 (024) 19:02:50.818	598706	9	0,200,300,300,300	103	5
6	1/26/2004 (026) 19:05:55.306	1400000	No Information	No Information	No Information	No Information
7	1/27/2004 (027) 19:14:07.184	663570	9	0,200,300,300,300	135	5
8	1/30/2004 (030) 19:03:39.905	785864	9	0,200,300,300,300	131	5
9	1/31/2004 (031) 19:03:34.068	1154250	9	0,200,300,300,300	124	5
10	2/02/2004 (033) 19:04:43.916	779986	9	0,200,300,300,300	93	5
11	2/06/2004 (037) 19:03:31.610	1400000	No Information	No Information	No Information	No Information
12	2/07/2004 (038) 19:38:09.849	332208	9	0,200,300,300,300	54	5
13	2/13/2004 (044) 21:03:27.024	849494	9	0,200,300,300,300	147	5
14	2/14/2004 (045) 19:03:05.358	338114	9	0,200,300,300,300	56	5
15	2/19/2004 (050) 19:07:30.699	1041470	9	0,200,300,300,300	234	5
16	3/04/2004 (064) 22:01:59.993	1355060	20	0,60	180	2
17	3/05/2004 (065) 19:03:46.035	2116185	9	0,200,300,300,300	292	5
18	3/05/2004 (065) 21:01:58.752	1289741	9	0,200,300,300,300	170	5
19	3/06/2004 (066) 19:06:00.406	1203848	20	0,60	124	2
20	3/10/2004 (070) 19:01:57.258	2208983	20	0,60	246	2
21	3/12/2004 (072) 19:38:12.515	749382	20	0,60	91	2
22	3/19/2004 (079) 22:12:47.802	1730324	20	0,60	265	2
23	4/03/2004 (094) 19:04:45.114	2044854	20	0,40,20	276	3
24	4/05/2004 (096) 20:04:06.626	1596457	20	0,60	277	2
25	4/06/2004 (097) 18:11:37.418	550017	20	0,60	108	2
26	4/16/2004 (107) 18:07:45.848	1454228	20	0,60	239	2
27	4/18/2004 (109) 18:04:06.976	1650858	20	0,60	447	2
28	4/19/2004 (110) 18:02:09.291	1400000	No Information	No Information	No Information	No Information
29	4/23/2004 (114) 21:11:50.503	1400000	No Information	No Information	No Information	No Information
30	5/19/2004 (140) 20:01:28.943	1123887	9	0,200,300,300,300	143	5
31	5/20/2004 (141) 18:04:53.535	1465606	9	0,200,300,300,300	178	5
32	5/21/2004 (142) 20:03:27.728	2462265	9	0,200,100,200,300,300	530	6
33	5/23/2004 (144) 18:06:58.214	1595365	9	0,200,300,300,300	182	5

Note that the interrow delay times are the delay times between successive rows. The total delay time between any two rows may be larger (e.g., for event 1, the delay time between rows 1 and 5 is 200 + 300 + 300 + 300 = 1100 msec).

taken as an "unknown" event and classified according to the class of events it is closest to (using the Mahalanobis distance as a measure of the separation). We can then evaluate the percentage of correctly classified events as our objective function. This is similar to the "drop-one event identification test" described in article 1 as an objective test for the methodology, but in this study we are using this method as part of the optimization procedure for evaluating optimum input parameters. The key improvement over the method used in article 1 is that the new method does not bias the event classification in favor of a particular group. Subsequently, there is no statistical reason why there should be a greater number of misclassified events from a particular group (as there was in article 1, which lead to an increased number of misclassified earthquakes).

Technique for Utilizing Array Data

Various methods can be used for incorporating the supplementary data from separate elements in an array. For our case there are two main schemes: (1) stacking of spectrograms at the individual array elements and (2) beamforming. In this article, we focus on the first of these methods, as it is the most effective way to enhance time-independent banding at all frequencies, while reducing the contribution from uncorrelated noise. This is because stacking the spectrograms reduces the spectral variance without the reduction of high-frequency amplitudes that occurs during beamforming. With beamforming, the signal coherence across the array diminishes for high frequencies, resulting in a loss of high-frequency signal energy (e.g., Taylor and Marshall, 1991).

The approach taken in this study is to evaluate a spec-

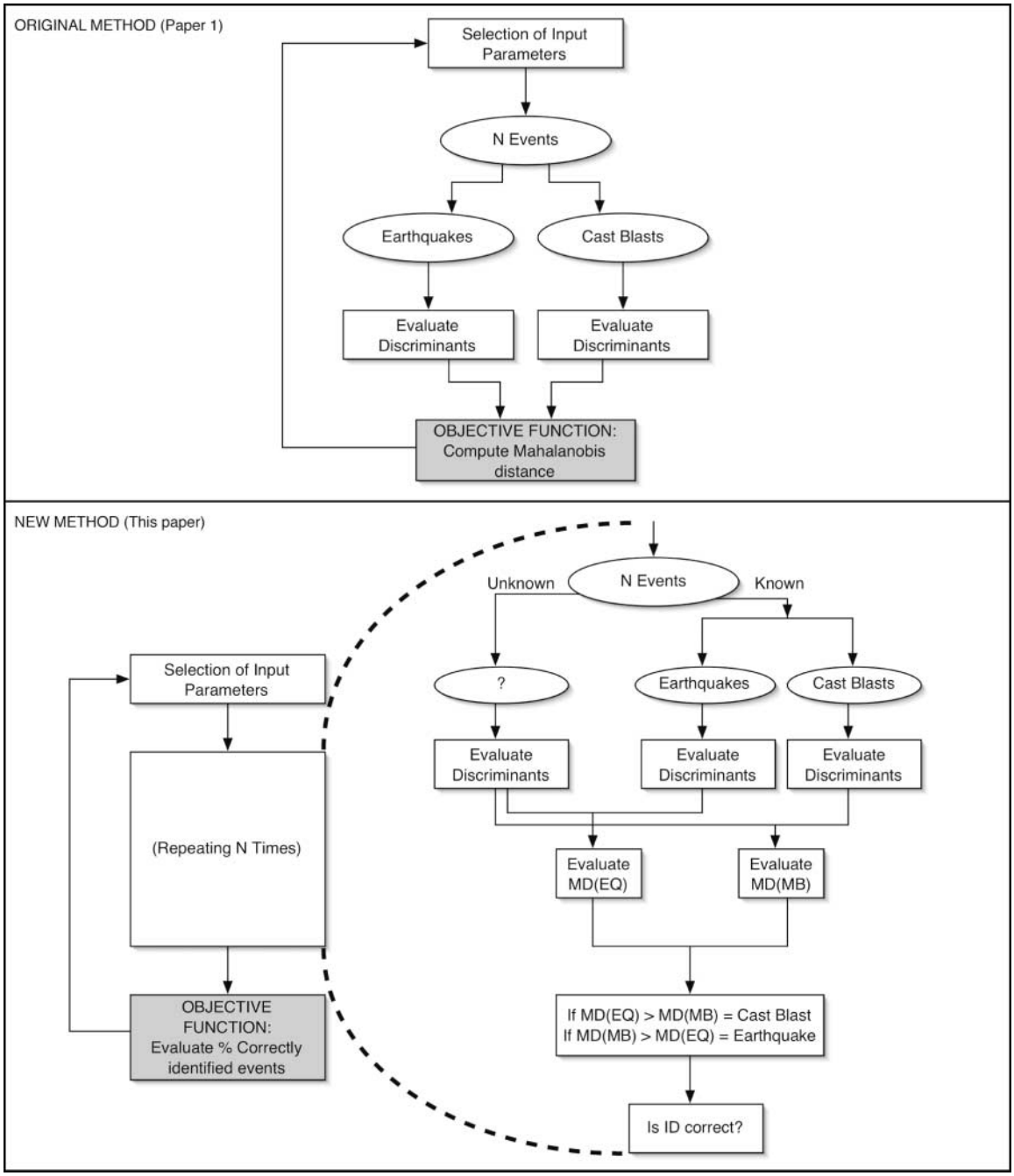

Figure 2. Flowcharts that illustrate the differences between the objective function used for optimizing the input parameters in article 1 (Mahalanobis distance), and the new objective function introduced in this article (percentage of correctly identified events). (Top) Method used in article 1. The objective function is evaluated by taking the mean Mahalanobis distance between all earthquake and cast blast discriminants (equation 3 in article 1). The mean Mahalanobis distance is evaluated separately for each selection of input parameters. (Bottom) Method used in this article. For each selection of input parameters we evaluate the percentage of events that are correctly classified. This metric (percentage of correctly classified events) is then the objective function that is optimized.

trogram for each element of the array separately and stack the spectrograms from all the array elements. Because each spectrogram is computed for a time window that begins at the picked first arrival at each array element, they can be stacked without the need for aligning based on the speed and direction of the incoming wavefront.

Dataset

The dataset we have used in this study comes from the Pinedale array (PDAR) in Wyoming (Fig. 3). We have chosen to apply our methodology to this dataset for three primary reasons: (1) we have developed a close relationship with a mining operator in the Powder River Basin and have obtained excellent ground truth on explosions (including shot type, yield, and origin time information); (2) the mine location is conveniently located ~360 km from PDAR, which has allowed us to study the improved discriminant performance that can be obtained using an array; and (3) there are a good number of sources of natural seismicity in this region. In article 1 we used data from only a single (broadband) element of the PDAR array, PD31. However, the PDAR array comprises 15 elements, of which 13 are single-component short-period seismometers, with one three-component short-period instrument and one three-component broadband instrument. With the exception of the single-broadband instrument (PD31), the sampling rate used is 20 Hz. Data from PD31, which are sampled at 40 Hz, are resampled to 20 Hz after low-pass filtering. There are five categories of events detonated at the Powder River Basin mine, which range in yield from 200 to 2.5 million lbs (article 1). Specific ground-truth information on the 33 cast blasts (the largest of the mining event types, which we focus on next) is tabulated in Table 1. Origin times and locations for regional earthquakes (Fig. 3) have been obtained from the U.S. Geological Survey (USGS) catalog and from earthquake catalogs compiled by the University of Utah and the Montana Bureau of Mines and Geology. In total, our dataset comprises 98 regional recordings of delay-fired mining explosions (of which 33 are cast blasts) and 43 recordings of regional earthquakes.

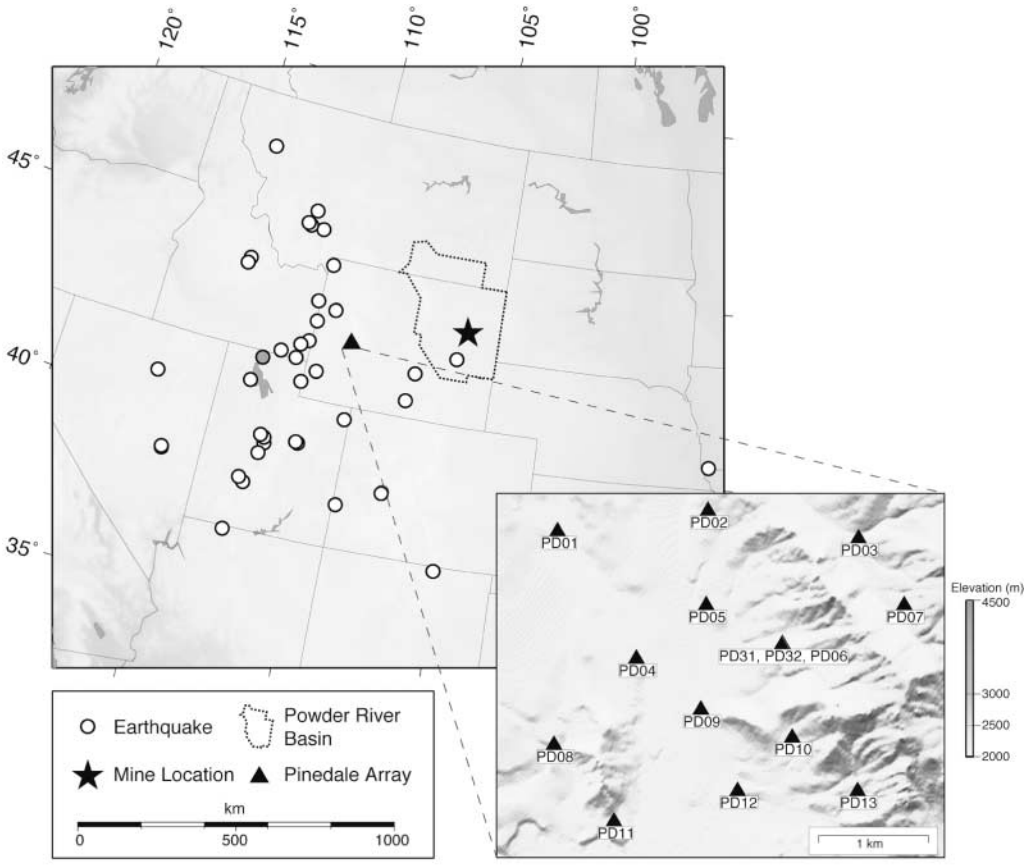

Figure 3. Location map of the study area showing the location of the PDAR seismic array (filled triangle), the mine location (filled star), and the locations of earthquakes in the dataset (circles). The location of the one misclassified earthquake is shown by the shaded circle; open circles represent the remaining earthquakes. (Inset) Detailed map of the PDAR seismic array showing the locations of the 15 separate sensors.

Results and Discussion

The values of the five input parameters have been optimized for a single short-period array element using the technique described in article 1 with the modifications described previously. The optimum parameters are the parameters that result in the highest percentage of correctly identified events (Fig. 2). Because of the difference in recording system (e.g., sampling rate), and the difference in the objective function used, the optimum input parameters are slightly different than those used in article 1. For simplicity, we have used the same input parameters for all short-period array elements and for the one broadband instrument in the PDAR array. The optimum input parameters are 150 sec for the spectrogram duration (w), 0.20 and 1.56 Hz for the averaging windows used in converting the spectrograms into binary form (*sp1* and *sp2*), 13 for the spectral amplitude threshold ($\propto$) used for removing noise comparable to the pre-event noise and 1 sec for the window over which the mean cepstral value is evaluated (cep). Using the full array stack with the noise-correction procedure described earlier, the optimum value of the objective function (percentage of correctly identified events) is 97.4%. A different choice of input parameters would result in an increase in the number of misclassified events. For example, for the arbitrary choice of sp1 = 0.5 Hz and sp2 = 1 Hz (with the other input parameters held at their optimum values), the percentage of correctly identified events is 88.2%. This results in the misclassification of nine events, rather than the two events that are misclassified when using the optimum input parameters. This illustrates the importance of the choice of input parameters, as discussed in more detail in article 1.

The four categories of smaller mining explosion detonated at the mine (with the exception of some truck-shovel [TS] overburden blasts) do not exhibit spectral modulation (article 1). This inability to discriminate the smaller explosions may be associated with the bandwidth of the data (discussed previously). The smaller shots are delay-fired events, but are shorter in duration and not typically associated with multiple rows of shots. It may be possible to discriminate these events based on the intershot delay times, but closer measurements (with a bandwidth $>$100 Hz) would be required. However, the fact that these smaller events do not exhibit spectral modulations indicates that the spectral modulations observed in the cast blasts are acquired by source processes, and not propagation effects (as observed by Sereno and Orcutt [1985]). This study will focus on the discrimination between earthquakes and cast overburden shots. However, the smaller mining explosions that do not exhibit spectral scalloping could effectively be considered to be part of the earthquake population in this study. In other words, the goal of this discrimination algorithm is to identify cast overburden shots from the composite set of events that includes earthquakes, single-fired shots, and the smaller mining explosions. Figures 4 and 5 show example spectrograms of three randomly selected cast overburden shots and three randomly selected earthquakes, respectively. In Figure 4, example spectrogram 1 corresponds to event 30 in Table 1, example 2 corresponds to event 12, and example 3 corresponds to event 32. In both Figures 4 and 5, the spectrograms are shown for (a) a single-array element (for comparison with the previous methodology described in article 1), (b) the full-array stack, and (c) the full-array stack after applying the noise correction method described previously. For the cast overburden shots (Fig. 4), it is clear that the binary spectrograms computed after array stacking (with no noise correction) exhibit significantly clearer time-independent spectral banding than for a single station. This demonstrates that we are clearly improving the signal-to-noise ratio, which supports our motivation for using the full array. After applying the noise-correction procedure described earlier, the binary spectrograms for the full-array stack continue to exhibit strong time-independent spectral banding. Because of the high signal amplitudes in this case, the noise correction only randomizes the binary spectrogram in the pre-event noise and at high frequencies at later times, where the signal amplitude is low. For the earthquakes (Fig. 5), the binary spectrograms computed after array stacking (with no noise correction) also exhibit more time-independent banding than for a single station in at least two cases (events 1 and 3 in Fig. 5). This is caused by the effect of time-independent noise that is coherent on all the array elements and is therefore summed in the array stack. By applying the noise correction, the time-independent banding observed in the earthquake spectrograms is largely cancelled out (Fig. 5).

Values of the two discriminants appropriate for single-component data (cepstral mean and autocorrelation) have been computed for each event. Three cases have been considered, which include a single station only (i.e., equivalent to the analysis performed in article 1), array stacking, and array stacking with noise correction (Fig. 6). For the single-station case, the values of the discriminants are within the single-station pre-event noise range for the earthquakes and smaller mine shots. However, numerous cast blasts are associated with discriminants above the single-station pre-event noise. The percentage of successfully identified events for the single-station case was 85.5% (i.e., a total of 65 of the 76 events, which include the earthquakes and cast blasts, were classified correctly). This result is similar to the result obtained using PD31 in article 1 (i.e., 89.5% of events correctly identified). Using the full array (with no noise correction applied), the values of the discriminants increase significantly for both the earthquakes (and smaller shots) and the cast blasts. However, the values of the discriminants for the earthquakes (and smaller shots) are still within the noise range, although the stacked noise range is much larger (Figs. 1 and 6). In this case, the percentage of successfully identified events was 97.4% (i.e., a total of 74 of the 76 events were classified correctly). The final case studied was full-array stacking with an additional noise correction (as described earlier). Here, the values of the discriminants for the earthquakes (and smaller shots) are decreased from the

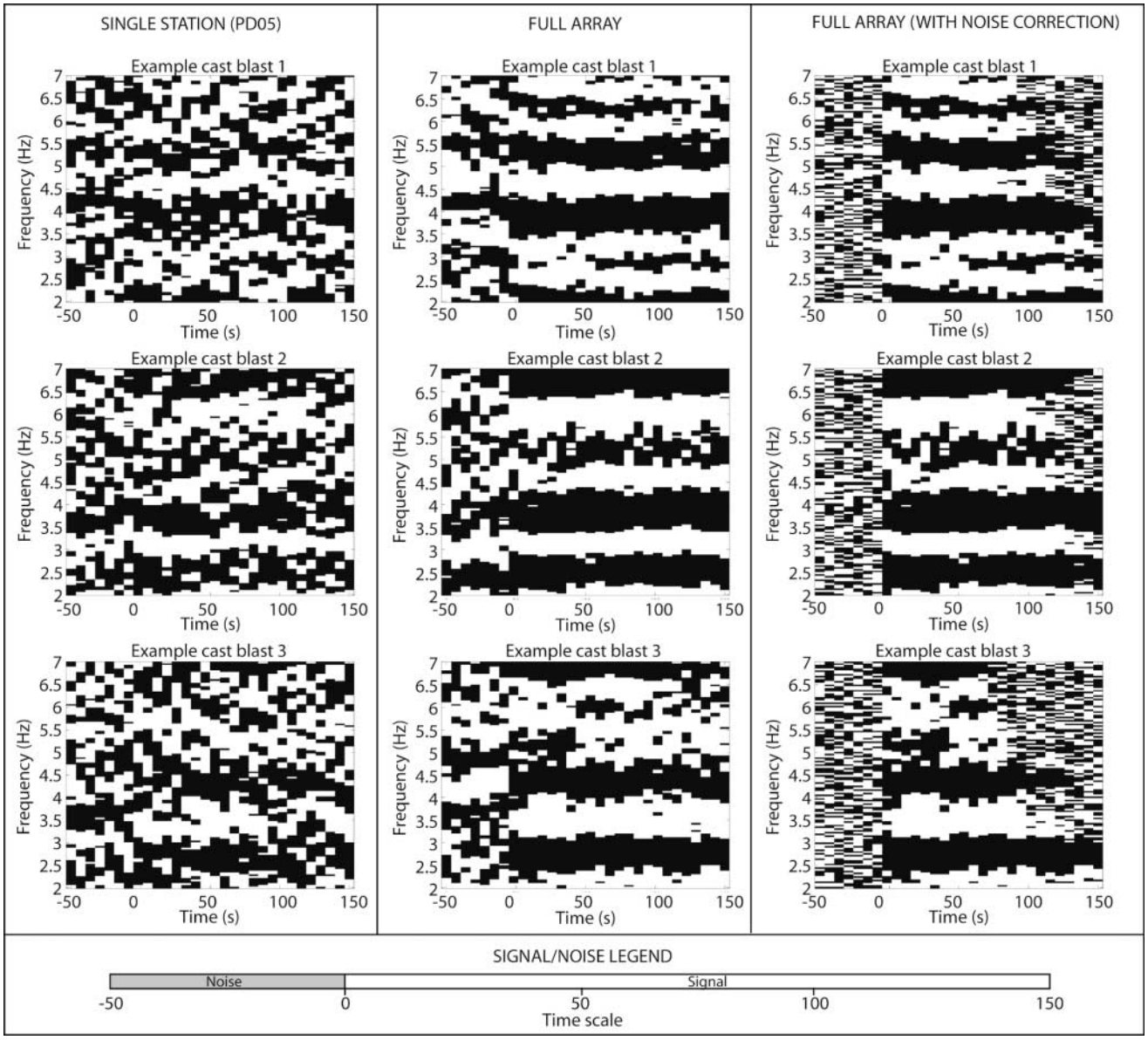

Figure 4. Binary spectrograms for three randomly chosen cast blasts, generated using a single station only (left column), the full-array stack (center column), and the full-array stack with an additional noise correction (right column). For each event, 50 sec of pre-event noise are included in the spectrogram for comparison. Zero time corresponds to the first arriving *P* wave. In each case, the binary spectrograms were determined by using the optimum set of input parameters.

full-array result and return to single-station noise levels. However, the discriminant values associated with the cast blasts are not decreased. The percentage of successfully identified events in this case was also 97.4%, but the mean Mahalanobis distance between the earthquake and cast blast groups is much greater after applying the noise correction than it was beforehand. The mean Mahalanobis distance is 92.6 for the noise-corrected array stack and 50.9 for the array stack with no noise correction. This shows that the noise correction improves the performance of the discriminant (i.e., the overall separation between the two event classes becomes larger), despite the fact that the percentage of successfully identified events is the same in both cases.

This result (97.4% of events are correctly classified) demonstrates that this methodology is very successful at identifying the cast blasts in this region and that using the full array significantly improves the result for a single station. We have investigated in detail the two events that were misclassified in the full-array result to learn why they were not correctly identified. The waveforms and corresponding binary spectrograms of the two events are shown in Figure 7. It is clear that the earthquake exhibits time-independent

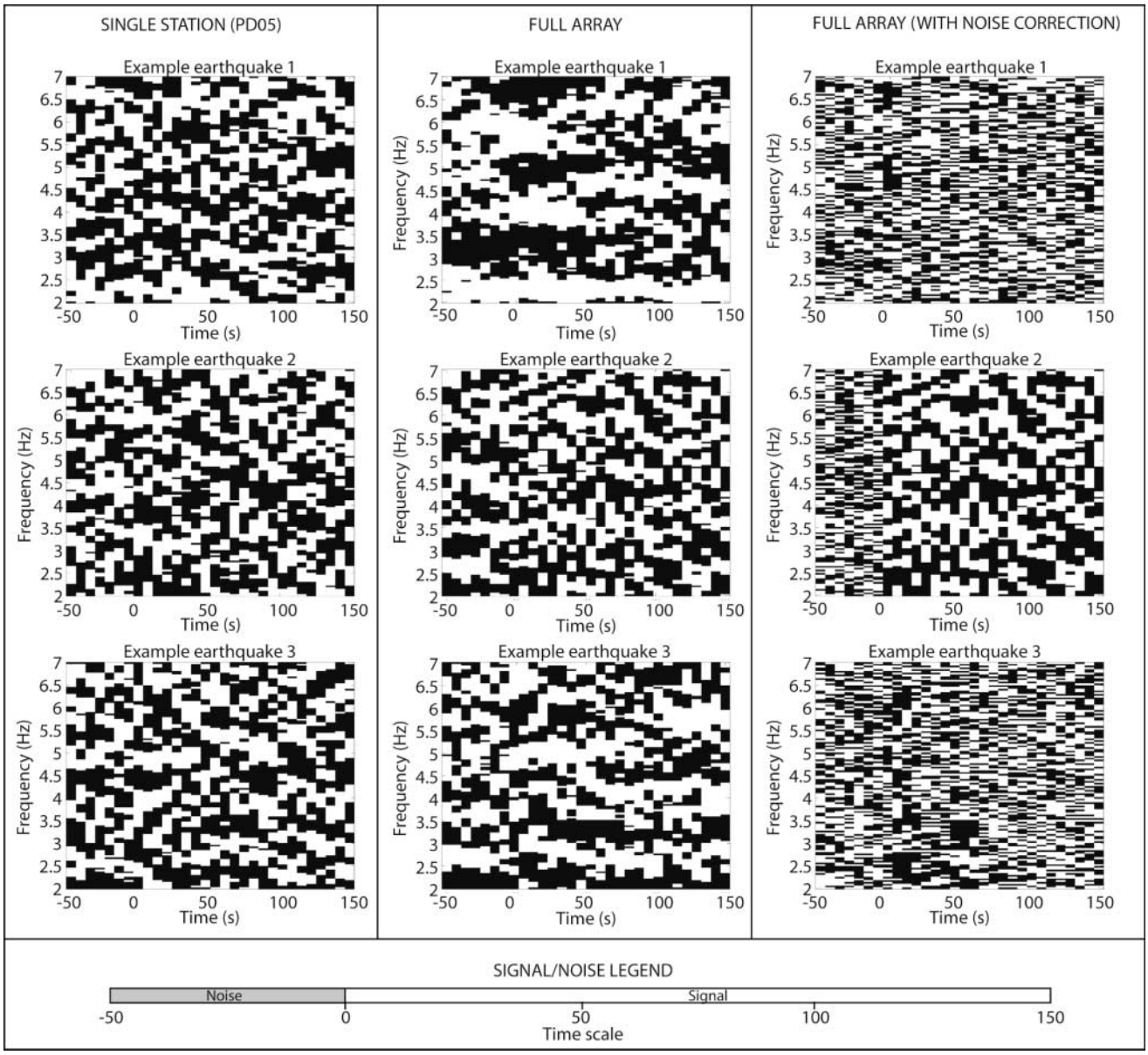

Figure 5. Binary spectrograms for three randomly chosen earthquakes, generated using a single station only (left column), the full-array stack (center column), and the full-array stack with an additional noise correction (right column). For each event, 50 sec of pre-event noise are included in the spectrogram for comparison. Zero time corresponds to the first arriving *P* wave. In each case, the binary spectrograms were determined by using the optimum set of input parameters.

spectral banding, although to a lesser degree than the spectral banding observed in typical cast blasts (Fig. 4). However, because of this spectral banding the earthquake is associated with discriminant values that place it in the explosion group. Conversely, the misclassified explosion exhibits no clear spectral banding and is associated with an essentially random binary spectrogram, consistent with a typical earthquake. It is possible that the earthquake, which was reported in the University of Utah catalog, is actually a cast overburden blast that was misclassified in the catalog. The University of Utah does not run a discrimination algorithm, but checks seismically derived locations with known mine locations and use contact persons at the mines for confirmation (Relu Barlacu, personal comm., 2006). The event in question had a well-constrained epicenter of (41.83° N, 112.68° W), depth of 1.4 km and magnitude (m_b) of 2.3 (Fig. 3). The epicenter is not in a known mining region, which suggests it is unlikely that the event is in fact a delay-fired mining explosion. To provide independent confirmation of the location reported by the University of Utah, we have performed

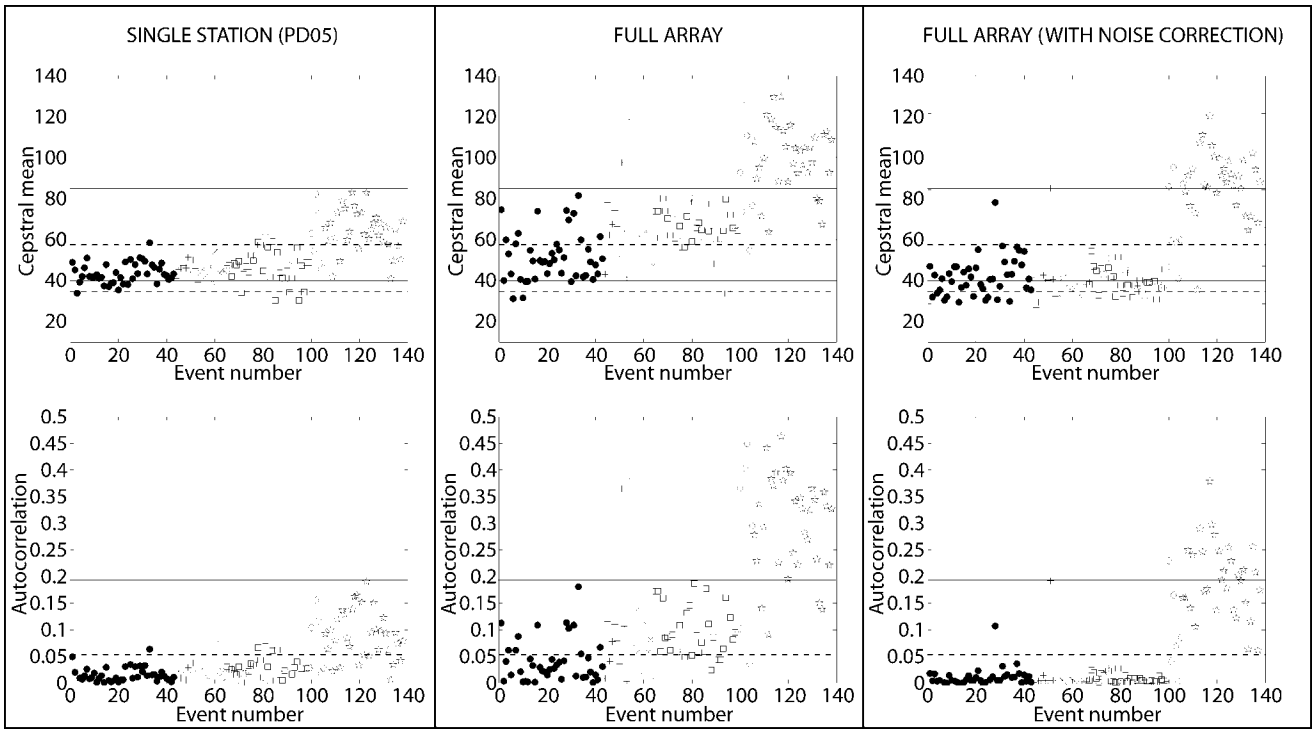

Figure 6. Values of the two discriminants (top row, cepstral mean; bottom row autocorrelation) obtained for each event using a single station only (left column), the full-array stack (center column), and the full-array stack with the noise correction applied (right column). In each case, filled circles represent earthquakes, plus signs represent parting shots, crosses represent coal extraction shots in the upper coal seam, open squares represent coal extraction shots in the main coal seam, open diamonds represent TS overburden blasts, and open stars represent cast overburden shots (refer to article 1 for more information on shot types). The solid lines show the extreme upper and lower bounds of discriminants evaluated from 50 samples of stacked pre-event noise spectrograms (using all 15 array elements). The dashed lines show the equivalent upper and lower bounds for a single-array element (i.e., without stacking).

an F-k analysis to confirm that the backazimuth of the recorded waveforms is consistent with the documented epicenter, and found a match within the estimated uncertainty. Therefore, this event appears to be a failure of this algorithm, but possibly would not have been misclassified if this method were used in conjunction with other regional waveform discrimination algorithms (e.g., correlation methods).

The misclassified explosion (event 8 in Table 1) may be due to the inaccurate documentation of the origin time (reported by the blast engineer at the mine). Indeed, the origin time reported by the blast engineer would imply an earlier arrival time (approximately 6 min earlier) than the recorded arrival time at PDAR. However, there were no consistent events in the data that would provide a closer match to the origin time reported by the blast engineer. Although 6 min is quite a significant time offset, it is not unusual in the case of this type of ground truth. This could be a problem if there were an approximately coincident regional earthquake that was the true source of the signal at PDAR. An F-k analysis, however, confirms that the backazimuth of the event is consistent with the true backazimuth of the mine. Since there are relatively few regional earthquakes at approximately this backazimuth (Fig. 3), it would seem unlikely (but not impossible) that the event was indeed an earthquake. The signal-to-noise ratio of the misclassified explosion is very low (Fig. 7) and this could be the cause of the event being misclassified.

Conclusions

The IMS network comprises a combination of seismic arrays and single stations. At present, most regional discrimination algorithms do not fully utilize the power of combining array elements and are therefore more applicable to single stations. The results presented in this article have shown how a time-frequency discrimination algorithm, developed in an earlier article, can be applied to seismic arrays to improve the success rate of source identification. We have also extended the method outlined in our previous article by developing a procedure for correcting for the effect of pre-event noise. We have shown how this procedure further improves the performance of the discrimination algorithm. Using the full PDAR array in Wyoming, the algorithm successfully identifies 74 of a total of 76 events, which comprise

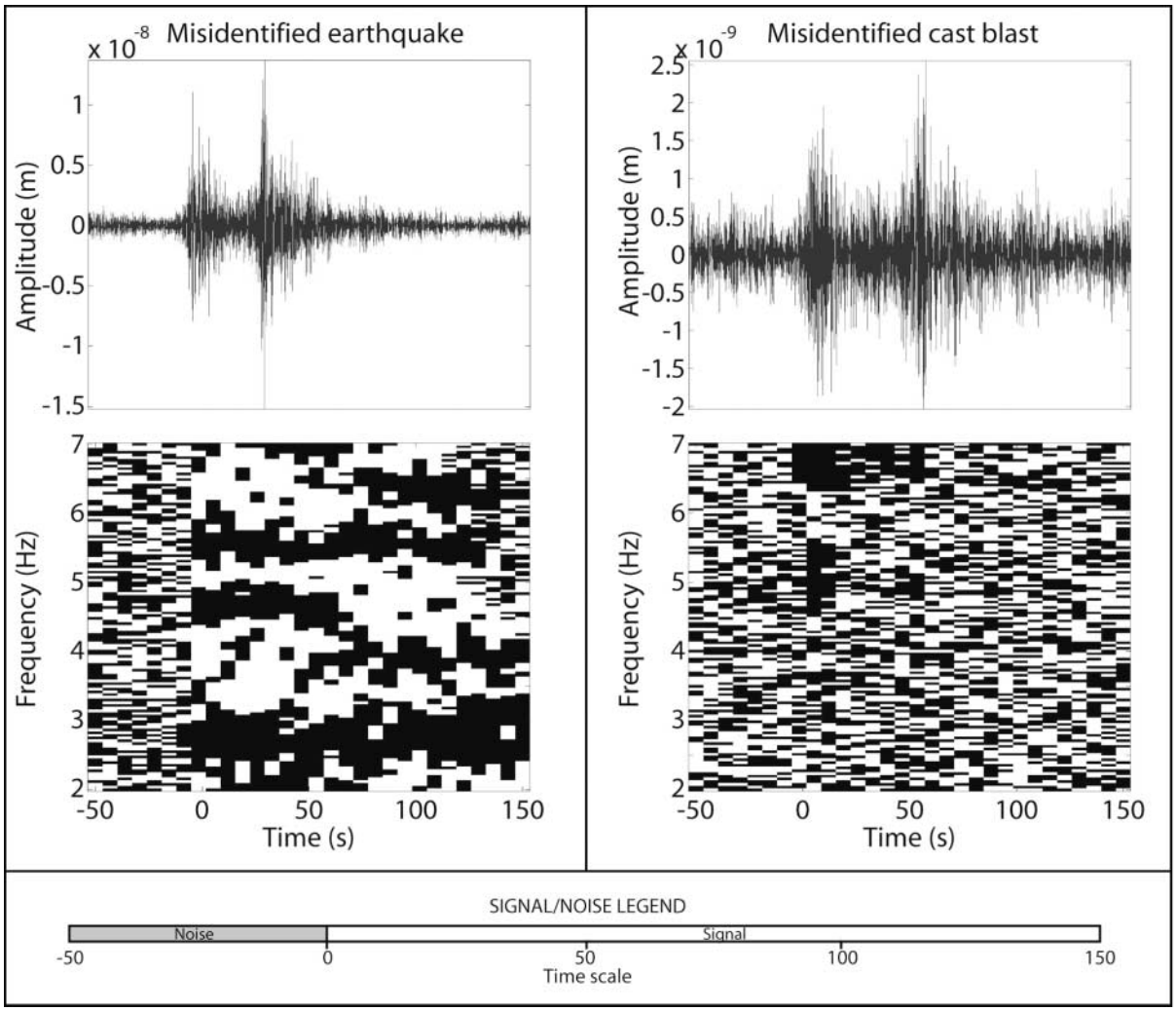

Figure 7. Waveforms and associated binary spectrograms of the two events that were misclassified using data from the full array. Note that the waveforms are taken from a single element of the PDAR array (PD05). For each event, 50 sec of pre-event noise are included in the spectrogram for comparison. Zero time corresponds to the first arriving *P* wave. The left-hand side shows the results for the misclassified earthquake and the right-hand side shows the results for the misclassified cast blast.

earthquakes and cast overburden blasts. This result illustrates the effectiveness of this technique and, in particular, the benefit derived from utilizing data from full arrays.

Acknowledgments

We thank Keith Koper, Yefim Gitterman, and one anonymous reviewer for their comments and suggestions that helped to improve this manuscript. We also thank Steve Beil at Arch Coal for providing mine shot information. This research was funded by NNSA contract numbers DE-FC52-03NA99510 and DE-FC52-03NA99511.

References

Arrowsmith, S. J., M. D. Arrowsmith, M.A.H. Hedlin, and B. Stump (2006). Discrimination of delay-fired mining events in Wyoming using an automatic time-frequency discriminant, *Bull. Seism. Soc. Am.* **96,** no. 6, 2368–2382.

Baumgardt, D. R., and G. B. Young (1990). Regional seismic waveform discriminants and case-based event identification using regional arrays, *Bull. Seism. Soc. Am.* **80,** 1874–1892.

Baumgardt, D. R., and K. A. Ziegler (1988). Spectral evidence for source multiplicity in explosions: Application to regional discrimination of earthquakes and explosions, *Bull. Seism. Soc. Am.* **78,** 1773–1795.

Bratt, S. R., and T. C. Bache (1988). Locating events with a sparse network of regional arrays, *Bull. Seism. Soc. Am.* **78,** 780–798.

Bungum, H., and E. S. Husebye (1974). Analysis of operational capabilities for detection and location of seismic events at NORSAR, *Bull. Seism. Soc. Am.* **64,** 637–656.

Cansi, Y. (1995). An automated seismic event processing for detection and location: the P.M.C.C. method, *Geophys. Res. Lett.* **22,** 1021–1024.

Chapman, M. C., G. A. Bollinger, and M. S. Sibol (1992). Modeling delay-fired explosion spectra at regional distances, *Bull. Seism. Soc. Am.* **82,** 2430–2447.

Douze, E. J., and S. J. Laster (1979). Seismic array noise studies at Roosevelt Hot Springs, Utah geothermal area, *Geophysics* **44,** 1570–1583.

Dysart, P. S., and J. J. Pulli (1990). Regional seismic event classification

at the NORESS array: seismological measurements and the use of trained neural networks, *Bull. Seism. Soc. Am.* **80,** 1910–1933.

Friedrich, A. A., F. A. Kruger, and K. A. Klinge (1998). Ocean-generated microseismic noise located with the Grafenberg array, *J. Seism.* **2,** 47–64.

Gitterman, Y., and T. Van Eck (1993). Spectra of Quarry Blasts and Microearthquakes Recorded at Local Distances in Israel, *Bull. Seism. Soc. Am.* **83,** 1799–1812.

Gitterman, Y., V. Pinsky, and A. Shapira (1998). Spectral classification methods in monitoring small local events by the Israel seismic network, *J. Seism.* **2,** 237–256.

Hedlin, M. A. H. (1998). A global test of a time-frequency discriminant, *Bull. Seism. Soc. Am.* **88,** 973–988.

Hedlin, M. A. H., J. B. Minster, and J. A. Orcutt (1989). The time-frequency characteristics of quarry blasts and calibration explosions recorded in Kazakstan, USSR, *Geophys. J. Int.* **99,** 109–121.

Hedlin, M. A. H., J. B. Minster, and J. A. Orcutt (1990). An automatic means to discriminate between earthquakes and quarry blasts, *Bull. Seism. Soc. Am.* **80,** 2143–2160.

Langefors, U., and B. Kihlstrom (1978). *The Modern Technique of Rock Blasting*, Wiley, New York.

Mykkeltveit, S., and F. Ringdal (1981). Phase identification and event location at regional distances using small-aperture array data, in *Identification of Seismic Sources—Earthquake or Underground Explosions*, E. S. Husebye and S. Mykkeltveit (Editors), NATO Advanced Study Institute Series, Dordrecht, The Netherlands, 467–481.

Ringdal, F., and E. S. Husebye (1982). Application of arrays in the detection, location, and identification of seismic events, *Bull. Seism. Soc. Am.* **72,** S201–S224.

Ringdal, F., E. S. Husebye, and A. Dahle (1975). P-wave envelope representation in event detection using array data, in *Exploitation of Seismograph Networks*, K. G. Beauchamp (Editor), Nordhoff-Leiden, The Netherlands, 353–372.

Sereno, T. J., and J. A. Orcutt (1985). Synthetic seismogram modeling of the oceanic Pn phase, *Nature* **316,** 246–248.

Shapira, A., Y. Gitterman, and V. Pinsky (1996). Discrimination of seismic sources using the Israel Seismic Network, in *Proceedings of the 18th Symposium on Monitoring a CTBT*, 612–621.

Shumway, R. H., D. R. Baumgardt, and Z. A. Der (1998). A cepstral F statistic for detecting delay-fired seismic signals, *Technometrics* **40,** 100–110.

Smith, A. T. (1989). High-frequency seismic observations and models of chemical explosions: implications for the discrimination of ripple-fired mining blasts, *Bull. Seism. Soc. Am.* **79,** 1089–1110.

Taylor, S. R., and P. D. Marshall (1991). Spectral discrimination between Soviet explosions and earthquakes using short-period array data, *Geophys. J. Int.* **106,** 265–273.

Withers, M. M., R. C. Aster, C. J. Young, and E. P. Chael (1996). High-frequency analysis of seismic background noise as a function of wind speed and shallow depth, *Bull. Seism. Soc. Am.* **86,** 1507–1515.

Institute of Geophysics and Planetary Physics
Scripps Institution of Oceanography
University of California
San Diego, California 92093-0225
sarrowsmith@gmail.com
hedlin@epicenter.ucsd.edu
(S.J.A., M.A.H.H.)

Department of Geological Sciences
Dedman College, Southern Methodist University
P.O. Box 750395
Dallas, Texas 75275-0395
plutonium@gmail.com
bstump@smu.edu
(M.D.A., B.S.)

Manuscript received 20 June 2006.